ACS APPLIED MATERIALS & INTERFACES

Research Article

www.acsami.org

# High Sulfur Loading Cathodes Fabricated Using Peapodlike, Large Pore Volume Mesoporous Carbon for Lithium−Sulfur Battery

Duo Li, Fei Han, Shuai Wang, Fei Cheng, Qiang Sun, and Wen-Cui Li*

State Key Laboratory of Fine Chemicals, School of Chemical Engineering, Dalian University of Technology, Dalian 116024, P. R. China

**ABSTRACT:** Porous carbon materials with large pore volume are crucial in loading insulated sulfur with the purpose of achieving high performance for lithium−sulfur batteries. In our study, peapodlike mesoporous carbon with interconnected pore channels and large pore volume (4.69 $cm^3$ $g^{-1}$) was synthesized and used as the matrix to fabricate carbon/sulfur (C/S) composite which served as attractive cathodes for lithium−sulfur batteries. Systematic investigation of the C/S composite reveals that the carbon matrix can hold a high but suitable sulfur loading of 84 wt %, which is beneficial for improving the bulk density in practical application. Such controllable sulfur-filling also effectively allows the volume expansion of active sulfur during $Li^+$ insertion. Moreover, the thin carbon walls (3−4 nm) of carbon matrix not only are able to shorten the pathway of $Li^+$ transfer and conduct electron to overcome the poor kinetics of sulfur cathode, but also are flexible to warrant structure stability. Importantly, the peapodlike carbon shell is beneficial to increase the electrical contact for improving electronic conductivity of active sulfur. Meanwhile, polymer modification with polypyrrole coating layer further restrains polysulfides dissolution and improves the cycle stability of carbon/sulfur composites.

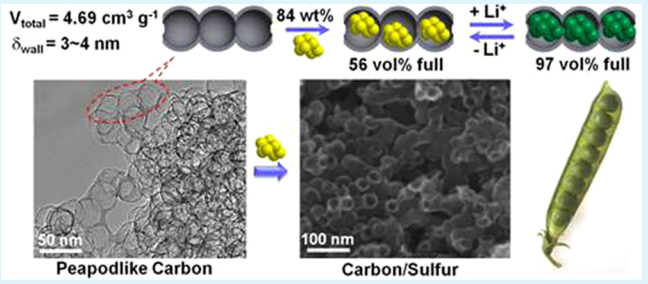


**KEYWORDS:** *lithium−sulfur battery, peapodlike mesoporous carbon, carbon/sulfur composite, large pore volume, high sulfur loading cathode*

## 1. INTRODUCTION

With the increasing demand of the world energy consumption, Li-ion batteries (LIBs) have been widely used as the primary electrical energy storage devices in various portable electronics for their lightweight relative to other types of batteries. However, LIBs are approaching the theoretical specific energy limits issues from traditional intercalation materials with the limited capacity of about 400 W h $kg^{-1}$ (e.g., $LiCoO_2$: 387 W h $kg^{-1}$).[1] So the new system is being sought for the next-generation batteries to provide high energy density and reduce cost factors. With a theoretical capacity of 1675 mA h $g^{-1}$, elemental sulfur has been considered as one of the most promising alternative cathode materials for green transportation.[2−4] In typical lithium−sulfur (Li−S) systems, elemental sulfur serves as the active cathode material and lithium metal as the anode. Sulfur undergoes reduction by lithium to generate a series of polysulfides $Li_2S_n$ ($8 \geq n \geq 2$) to ultimately form $Li_2S$ during discharge.[5,6] In addition to the high capacity, utilization of sulfur as a cathode material has the advantages of natural abundance, low cost, and environmental friendliness.[7] Therefore, the Li−S battery shows great potential for the next generation of lithium batteries that are capable of offering high energy density as power sources for electric vehicles.[8,9]

However, the Li−S battery systems investigated previously have some persistent problems.[10−13] First, active sulfur faces to the low utilization and poor rate capability, due to the highly insulating nature sulfur ($5 \times 10^{-30}$ S $cm^{-1}$ at 25 °C). Second, $Li_2S$ and other insoluble compounds are generated and cover the active compounds during cycling, which inhibit access of lithium ions. Third, the dissolved polysulfides ($Li_2S_n$) diffuse through the electrolyte to the lithium anode where they are reduced to form solid precipitates such as $Li_2S_2$ or $Li_2S$. These reduced products can also diffuse back to the cathode by charging, leading to severe "shuttle phenomenon".

To overcome these problems, many attempts have been made, which focus on enhancing the electrical conductivity of the cathode and suppressing the loss of soluble polysulfide intermediates during cycling.[14,15] Many types of carbon materials have been developed as the matrix for preparation of carbon/sulfur (C/S) composites, such as carbon nanotube,[16,17] carbon fiber,[18,19] porous carbon,[20−22] carbon spheres,[23−25] and graphene.[26−29] Besides, conductive polymers are also introduced in Li−S cathode, like polymer/sulfur composites[30,31] or carbon/sulfur composites coated with polymers.[32,33] On the basis of the aforementioned studies, it is evident that porous carbon/sulfur composites, especially for mesoporous carbon, can yield a much improved electro-

Received: January 6, 2013
Accepted: March 2, 2013
Published: March 2, 2013

  

chemical activity and cycling stability. However, the small pore volume makes it hard to achieve a sulfur loading of >70 wt % and limits the available battery volume.[3] Therefore, the application of large pore volume carbon matrix with optimized pore structure is a new and promising approach for Li−S batteries.

In this paper, peapodlike mesoporous carbon, combining the advantages of large pore volume (4.69 $cm^3\ g^{-1}$) and bimodal mesopores (2 and 22 nm) structure, was synthesized by hard-template method using poly(benzoxazine)[34,35] as precursor and colloidal silica spheres as hard templates. Subsequently, elemental sulfur was impregnated into the mesoporous channels of carbon matrix through a melt-diffusion method with optimized sulfur contents. Because of the large pore volume and suitable pore size, the effective loading of active sulfur can be as high as 84 wt %. Beyond that, the peapodlike structures may display a good electrical conductivity through trapping and connecting these small sulfur particles, which are also flexible to warrant structure stability. Further coating a conducting layer of polypyrrole on the surface of the C/S composites would further enhance the cycle stability and high-rate discharge capacity of the Li−S battery.

## 2. EXPERIMENTAL SECTION

**2.1. Chemicals.** Resorcinol (99.5%) was purchased from Tianjin Kermel Chemical Reagent Co., Ltd. Ludox AS-40 was purchased from Sigma-Aldrich. Formaldehyde (37 wt %), 1,6-diaminohexane (DAH, 99.0%), sublimed sulfur (99.5%), hexadecyl trimethyl ammonium bromide (CTAB, 99.0%), iron(III) chloride hexahydrate ($FeCl_3{\cdot}6H_2O$, 99.0%), and pyrrole (98%) were supplied by Sinopharm Chemical Reagent Co., Ltd.

**2.2. Material Preparation.** *Synthesis of Peapodlike Mesoporous Carbon.* The mesoporous carbon was prepared using colloidal silica spheres as hard templates. Typically, resorcinol (0.220 g) was first dissolved in deionized water (100 g) with vigorous stirring at the temperature of 24 °C and then formaldehyde (37 wt %, 292 mL) and Ludox AS-40 (1.2 mL) were added to form a clear solution. After addition of DAH (0.058 g), the clear solution turned white immediately. The resultant solution was further heated to 80 °C accompanied with vigorous stirring 42 h. The obtained silica/polymer compounds were pyrolyzed at 800 °C under nitrogen atmosphere. Then the mesoporous carbon was obtained after the removal of the silica template with aqueous NaOH solution.

*Synthesis of Carbon/Sulfur Composites.* The C/S composites were prepared following a melt-diffusion strategy. The mass ratios of mesoporous carbon and sulfur were 1: 6; 1: 4; 1: 2.5, and the obtained C/S composites were accordingly denoted C/S-1, C/S-2, and C/S-3 respectively. Then the powder was ground and heated to 155 °C under argon gas for 6 h. This treatment lowers the viscosity of sulfur, thereby improving the sulfur distribution inside the C/S via capillary action. Then, the temperature was increased to and kept at 300 °C for 1 h to vaporize the superfluous sulfur on the outer surface of mesoporous carbon.

*Synthesis of the Polypyrrole-Coated C/S Composite.* The polypyrrole-coated composite was synthesized by an in situ chemical oxidative polymerization of pyrrole on C/S composite. First, C/S composite was dispersed in 50 mL water with 0.1 M CTAB by sonication for 0.5 h. Then, pyrrole was dropped into the solution and stirred for 30 min by magnetic stirring. After that, proper amount of $FeCl_3{\cdot}6H_2O$ (three times as much as the mole of the pyrrole) was added by dropping and stirred for 4 h. The product was washed and filtered until the filtrate was colorless. The composite was dried at 50 °C for 12 h. The mixture was then heated to 300 °C for 2 h under an argon atmosphere. Finally, the product was obtained after the system was naturally cooled to room temperature, and the obtained polypyrrole-coated composite was accordingly denoted as C/S@PPy.

**2.3. Structure Characterization.** X-ray diffraction patterns (XRD) were obtained with a D/MAX-2400 diffractometer using Cu $K_\alpha$ radiation (40 kV, 100 mA, $\lambda$ = 1.54056 Å). Nitrogen adsorption isotherm was measured at 77 K with an ASAP 3000 adsorption analyzer (Micromeritics). The Brunauer−Emmett−Teller (BET) method was utilized to calculate the specific surface areas. Pore size distribution (PSD) was derived from the adsorption branch of the isotherms using the Barrett−Joyner−Halenda (BJH) model. Total pore volumes were calculated from the amount adsorbed at a relative pressure, $P/P_0$ of 0.99. Elemental analysis was carried out on an elemental analyzer (Vario EL III, Elementar). The IR spectrum was collected on a Nicolet 6700 FTIR spectrometer. Scanning electron microscopy (SEM) was carried out with a FEI Nova NanoSEM 450 instrument at 10 kV. Transmission electron microscopy (TEM) analyses were carried out with a Tecnai $G^2$20S-Twin equipment operating at 200 kV. The sample for TEM analysis was prepared by dropping an ethanol droplet of the products on carbon-coated copper grids and drying at room temperature. Thermogravimetric analysis was measured from 25 to 500 °C with a heating rate of 10 °C $min^{-1}$ under nitrogen flow, using a STA449 F3 Jupiter thermogravimetric analyzer (NETZSCH).

**2.4. Electrochemical Characterization.** Electrochemical experiments were performed via CR2025 coin-type test cells assembled in an argon-filled glovebox with lithium metal as the counter and reference electrodes at room temperature. The cathode for Li−S batteries was prepared by mixing 80 wt % composite materials, 10 wt % carbon black and 10 wt % polyvinylidene difluoride (PVDF) in N-methyl-2-pyrrolidone (NMP) to form a slurry. Subsequently, the slurry was pasted onto a carbon-coated aluminum foil and Celgard 2400 membrane was used as the separator to isolate electrons. The electrolyte was 1 M bis(trifluoromethane) sulfonimide lithium salt (LiTFSI) dissolved in a mixture of 1,3-dioxolane (DOL) and dimethoxymethane (DME) (1:1 by volume). The discharge/charge measurements were conducted at a voltage interval of 1.0 to 3.0 V using a Land CT2001A battery test system at 0.2C (1C = 1675 mA $g^{-1}$). Cyclic voltammetry (CV) measurements were performed on CHI660D electrochemical workstation at a scan rate of 0.2 mV $s^{-1}$.

## 3. RESULTS AND DISCUSSION

**3.1. Structure and Morphology of the Mesoporous Carbon and C/S Composites.** As shown in Figure 1a, the nitrogen sorption isotherm was measured to determine the pore structure of the peapodlike mesoporous carbon material.

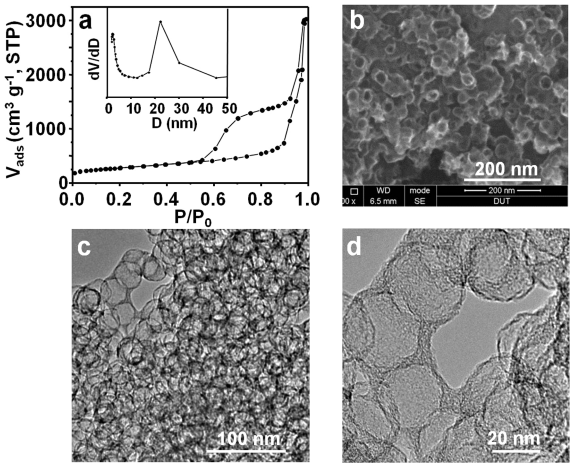


**Figure 1.** (a) Nitrogen sorption isotherm of the peapodlike mesoporous carbon. The inset is the corresponding pore size distribution calculated using the BJH formula from the adsorption branch. (b) SEM image of the peapodlike mesoporous carbon. (c, d) TEM images of the peapodlike mesoporous carbon.

The isotherm feature hysteresis between desorption and adsorption branches indicates the presence of mesopores.[36] The pore size distribution plot specifically confirms that the sample has a bimodal pore system concentrated at 22 and 2 nm, which are attributed to the diameter of silica spheres templates and the pores in the carbon walls, respectively. During the melt-diffusion process, the small mesopores (2 nm) in the carbon walls are in favor of liquid sulfur diffuse. Consequently, the large mesopores (22 nm) would serve as reservoirs for storing the sulfur. TEM images (Figure 1c, d) show that the mesoporous channels are interconnected, which is consistent with the SEM observation (Figure 1b). Previously, Wan et al. have confirmed the truth that the nanoporous carbon with interconnected nanochannels and thin walls is characteristically good conducting networks for both $Li^+$ and $e^-$.[37] Besides, the flexible elasticity of the carbon host effectively mitigates the structural degradation caused by the volume expansion upon full lithiation.[3]

The employed peapodlike mesoporous carbon in this study showed a high BET specific surface area of 977 $m^2\ g^{-1}$ and a large total pore volume of 4.69 $cm^3\ g^{-1}$, suggesting excellent potential for sulfur encapsulation. It was known that 1.0 g mesoporous carbon can accommodate 7.785 g of $Li_2S$ (1.66 g $cm^{-3}$ × 4.69 $cm^3\ g^{-1}$, that is the density of $Li_2S$ multiplied by the pore volume of the mesopores carbon), which corresponds to a maximum of 5.433 g sulfur obtaining a sulfur percentage of 84.5 wt %.[14] To investigate the effect of the sulfur loading, we conducted a series of experiments as follows. By precisely regulating the mass ratio between carbon materials and sulfur, we can determine the sulfur loading of the composites after melt-diffusion. Therefore, three samples C/S-1, C/S-2 and C/S-3 accordingly with 84, 77, and 60 wt % sulfur loading, were achieved, and the loadings of sulfur in the resultant C/S composites were proved by elemental analysis and TG analysis (Figure 2a). Among the three samples, C/S-1 (84 wt %) has the highest sulfur loading which is almost identical as the above-mentioned theoretical maximum value (84.5 wt %).

The XRD patterns before and after sulfur incorporation (Figure 2b) is a proof of good dispersion of sulfur in the C/S-1 composite which has the highest sulfur loading among the three samples. The broad signal around 24° mainly results from amorphous carbon. An XRD analysis of elemental sulfur (JCPDS: 08−0247) showed two prominent peaks at $2\theta$ = 23 and 28° that correspond to an $F_{ddd}$ orthorhombic structure,[38] which could also be seen in the C/S composites before sulfur melting (Figure 2b, blue curve) and disappeared in C/S composites after sulfur diffusion (Figure 2b, red curve), suggesting that the sulfur is well dispersed in the pores of peapodlike mesoporous carbon. Electron microscopy has been introduced to visually observe the morphology of carbon/sulfur composites. Both SEM and TEM images show negligible morphology change after sulfur loading, suggesting that sulfur is homogeneously distributed into the pores and that no obvious large sulfur agglomeration is observed.

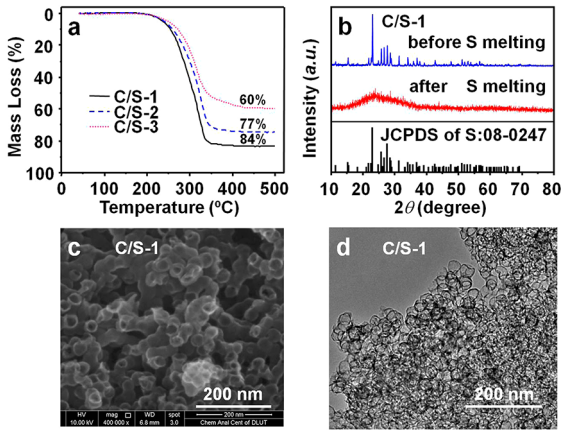


**Figure 2.** (a) TG curves of the C/S composites. (b) XRD patterns of C/S composite before and after melting diffusion. SEM (c) and TEM (d) images of C/S-1 composite.

**3.2. Electrochemical Performances of C/S Composites.** To check the electrochemical properties of C/S composites, the cyclic voltammogram (CV) and galvanostatic discharge−charge measurements were conducted for C/S-3 as a typical example. As shown in Figure 3a, the peak at 2.10 V (vs. $Li^+$/Li) corresponds to the conversion from elemental sulfur ($S_8$) to lithium polysulfide anions ($Li_2S_n$, where $n$ is typically 4−6). Another main peak is clearly identified at about 1.76 V during the first cathodic scan, which can be attributed to the deep reduction of polysulfide ions to insoluble $Li_2S_2$/$Li_2S$.[39] On the other hand, the two expected oxidation peaks overlap and form one large peak at about 2.69 V during the first anodic scan. This overlap may be due to high overpotential for conversion of $Li_2S$ to lithium polysulfide. However, the real reactions on the electrodes are more complicated than the typical electrochemical reactions, because of disproportionation reactions of the intermediate polysulfides during the charge/discharge process. Therefore, the reduction and oxidation peak areas are not one-to-one and do not correspond to that as expected for a conventional battery system.[26] In the subsequent scan, the main reduction peaks are shifted to higher potentials and the oxidation peaks to lower potentials. This potential shifting is mainly ascribed to the formation of complexes with lower adsorption energy after the first anodic oxidation of $Li_2S_n$, which indicates an improvement of reversibility of the electrode with cycling. Figure 3b shows charge/discharge voltage profile of C/S-3. The discharge curve shows two typical plateaus like all the sulfur-containing electrodes, which could be assigned to a two step reaction of sulfur with lithium during the discharge process, agreeing well with the results of CV measurements.

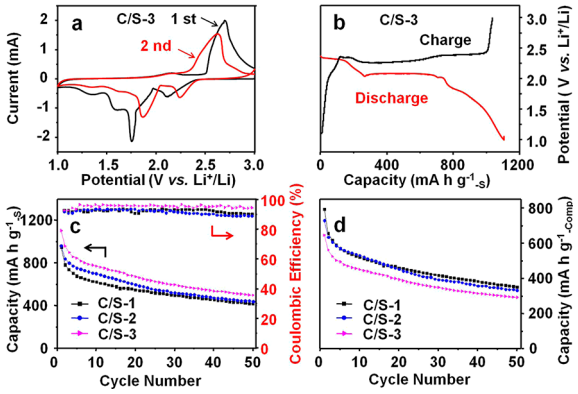


**Figure 3.** (a) Cyclic voltammogram of C/S-3 electrode at a sweep rate 0.2 mV $s^{-1}$. (b) Charge/discharge curve of the C/S-3 at a 0.2$C$ rate (1$C$ = 1675 mA $g^{-1}$) between 1.0 and 3.0 V vs Li/$Li^+$. Discharge capacities vs cycle numbers and Coulombic efficiency of the C/S composites based on (c) the mass of the sulfur and (d) the C/S composites at 0.2$C$ rate.

To illustrate the good properties of the C/S composites, we used two methods to calculate the specific capacity: one is based on the mass of the sulfur and the other one is based on the whole C/S composites. The specific capacities are plotted versus cycle numbers, as displayed in panels c and d in Figure 3, respectively. As seen in Figure 3c, composite C/S-3 with the sulfur loading of 60 wt %, has the highest specific capacity of the initial discharge among the three samples. The capacity was as high as 1106 mA h $g^{-1}$, which was about 66% of sulfur utilization based on the theoretical value (1675 mA h $g^{-1}$) of sulfur. It has been well accepted for Li−S battery that the initial discharge capacity usually declines with the increase of sulfur loading.[13] As the sulfur loading increased from 77 wt % (C/S-2) to 84 wt % (C/S-1), the capacities of C/S composites reached almost the similar value after 50 cycles, accompanying a similar fading tendency in capacity.

As the cathode contains two components, namely carbon and sulfur, but only sulfur offers capacity, so that the calculated capacities of the electrode are usually based on the mass of sulfur itself. In fact, considering a practical application, we also need to calculate the energy density of a battery based on the overall mass of the composites. Therefore, we introduce another calculating method that is based on the mass of the entire composites. If the formula of Figure 3c is defined as eq 1

$$\mathrm{Cap}_{-S} = \frac{Q}{m_{\mathrm{sulfur}}} \quad (1)$$

Where $\mathrm{Cap}_{-S}$ represents the specific discharging capacity of per cycle on the basis of the mass of sulfur, $Q$ is the total capacity stored in the electrode, and $m_{\mathrm{sulfur}}$ indicates the mass of sulfur. So the formula of Figure 3d could be defined as eq 2

$$\mathrm{Cap}_{-C} = \frac{Q}{m_{\mathrm{composite}}} \quad (2)$$

Where $\mathrm{Cap}_{-C}$ is the specific discharging capacity of per cycle based on the mass of the composites, and $m_{\mathrm{composite}}$ is the mass of sulfur. On the basis of eqs 1 and 2, the relationship between $\mathrm{Cap}_{-S}$ and $\mathrm{Cap}_{-C}$ is $\mathrm{Cap}_{-C} = \mathrm{Cap}_{-S} \times$ sulfur content (%).

From Figure 3d, the capacity of the C/S-1 with the highest sulfur loading is the largest among the three samples. This may set a way to construct suitable carbon matrix for practical application. Carbon with large pore volume is beneficial for reserving sufficient amount of active sulfur, meanwhile, the pores should show excellent interconnectivity, which facilitates the rapid ionic diffusion and electronic transport due to drastically shorten transport distance, thus exhibit better rate capability. However, like many other studies,[13,29] all C/S composites had the phenomenon of capacity fading, which was caused by the dissolved polysulfides ($Li_2S_n$).

**3.3. Electrochemical Performances of C/S@PPy Composite.** To further restrain the dissolution of polysulfide and improve the sulfur utilization, we purposively introduce conductive polymer, polypyrrole (PPy), as the coating layer for surface modification.[40] Figure 4d shows the FTIR spectra of mesoporous carbon and C/S@PPy composite. The characteristic bands of the C/S@PPy sample were consistent with data in literature.[41] The pyrrole ring fundamental vibration are at 1585 and 1505 $cm^{-1}$, the =C−H in-plane vibration are at 1250 and 1090 $cm^{-1}$, and the C−N stretching vibration is at 1180 $cm^{-1}$. Essentially, the molecular structure of the PPy chain prepared here is identical to that of the PPy synthesized using a common method. A slight difference may result from that a small amount of elemental sulfur reacts with polypyrrole to form a cross-linked S-PPy net. At a result, the sulfur has been both physically and chemically confined in the C/S@PPy composite.[23]

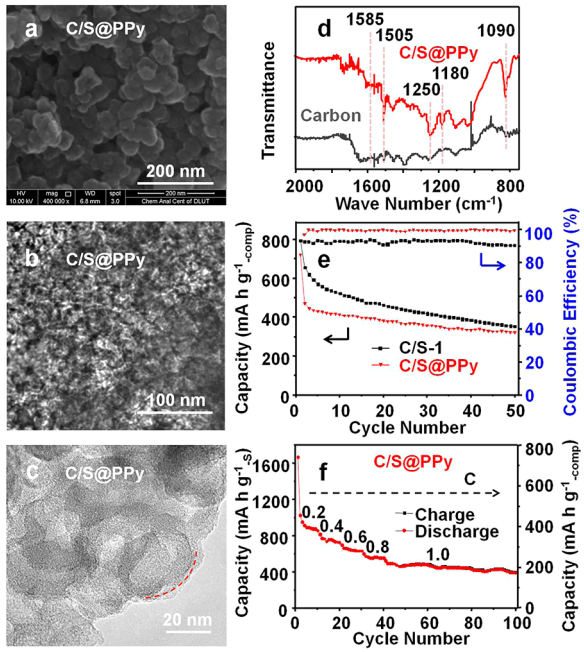


**Figure 4.** (a) SEM image of C/S@PPy composite. (b), (c) TEM images of C/S@PPy composite. The PPy layer was indicated by the red dashed line in 4c. (d) FT-IR spectra of mesopores carbon (gray) and the C/S@PPy composite (red). (e) Discharge capacities vs cycle numbers and Coulombic efficiency of C/S-1 and C/S@PPy composites based on the mass of the composite at 0.2 C rate. (f) Rate capability of the C/S@PPy composite based on two calculating methods.

In the C/S@PPy composite, the PPy-coated layer was supposed coating on the surface of the C/S composite. As seen in Figure 4a−c (SEM and TEM images of the C/S@PPy), it was clear to observe the evident morphology change as compared to that of the pristine C/S composite. For clarity, the PPy layer was indicated by the red dashed line in Figure 4c. Such a "layer-coated" structure in the C/S@PPy composite would further enhance the electrochemical performance of the composite by preventing lithium polysulfides from dissolving into the electrolyte. The discharge capacities of C/S@PPy and C/S-1 based on the mass of the composites are shown in Figure 4e. Because of the reduced sulfur loading, C/S@PPy shows a lower capacity than C/S-1 during the first several cycles. Importantly, C/S@PPy shows much higher stability than the C/S composite, that is stemmed from the PPy-coating layer restraining shuttle phenomenon. The rate capability of the C/S@PPy composite is shown in Figure 4f. The capacity gradually decreased as the current rate increased from 0.2 to 1 C. A satisfactory capacity of 400 mA h $g^{-1}$ based on the mass of sulfur was obtained for C/S@PPy at 1 C after 60 cycles.

**3.4. Effect of the Sulfur Loading and Surface Modification on Cycle Stability.** To further study the relationship between the electrochemical performance and the sulfur loadings, we introduce the capacity fading rate $f_c$. The $f_c$ is defined as eq 3[42]

$$f_c = \frac{C_1 - C_n}{n} \quad (3)$$


dx.doi.org/10.1021/am4000535 | ACS Appl. Mater. Interfaces 2013, 5, 2208−2213

Where $C_1$ and $C_n$ are the specific discharging capacities of first and $n^{th}$ cycle, and $n$ is the number of cycles. It has been known that the Li−S battery has poor electrode rechargeability owing to the insulating nature of sulfur and the solid reduction products ($Li_2S$ and $Li_2S_2$). We thus choose the second cycle as the point to calculate the capacity fading and the realistic formula is defined as eq 4

$$f_c = \frac{C_2 - C_n}{n - 1} \quad (4)$$

Where $C_2$ and $C_n$ are the specific discharging capacities of second and $n$th cycle, and $(n - 1)$ is the number of cycles.

The capacity fading rates of the composites were shown in Figure 5, it is obvious that the capacity fading rate of C/S composites gradually increases with the increase of sulfur loading. The fading rates of C/S-1, C/S-2, and C/S-3 are accordingly 6.22, 6.19, and 5.51 mA h $g^{-1}$ per cycle. We thus can establish a correlation between the fading rate and the sulfur loadings, as shown in Figure 5. Based on this correlation, the calculated fading rate was 5.00 mA h $g^{-1}$ per cycle, in the case of 43 wt % sulfur loading. In contrast, the fading rate of C/S@PPy is 3.05 mA h $g^{-1}$ per cycle, which indicates C/S@PPy is much stable as compared to the C/S composite. The PPy-coated layer can enhance, to some extent, the electrochemical performance of the composite by preventing lithium polysulfides to dissolve into the electrolyte.

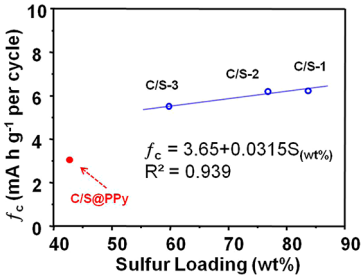


**Figure 5.** Correlation of the capacity fading rate $f_c$ and the different sulfur loadings. The blue hollow cycles represent C/S composites, and the red solid cycle represents C/S@PPy sample.

## 4. CONCLUSIONS

In this study, peapodlike mesoporous carbon with large pore volume (4.69 $cm^3$ $g^{-1}$) was used as a conducting matrix to encapsulate sulfur as Li−S battery cathodes. The sulfur loading can reach as high as 84 wt % on the basis of elemental analysis and TG measurement, owing to the large pore volume of the carbon host. Meanwhile, the flexible character of the carbon host effectively mitigates the structural degradation caused by the volume expansion upon full lithiation. Simultaneously, surface modification can enhance the stability of the composites by trapping the polysulfides formed during redox process. The sulfur loading and surface modification affect the electron and mass transfer during cycles, thus impact the performance of Li−S batteries. Further exploration focuses on a multifunctional composite with continuous peapodlike carbon network, high sulfur loading and conductive polymer coating would be beneficial for Li−S battery in practical application with desired capacity, high-rate capability, as well as cycle stability. Follow-up work of our group is under way.

## AUTHOR INFORMATION

### Corresponding Author

*Fax/Tel: (+86)-411-84986355. E-mail: wencuili@dlut.edu.cn.

### Notes

The authors declare no competing financial interest.

## ACKNOWLEDGMENTS

The project was supported by the Fundamental Research Funds for the Central Universities (DUT12ZD218), and the Ph.D. Programs Foundation (20100041110017) of Ministry of Education of China.

## REFERENCES

(1) Bruce, P. G.; Hardwick, L. J.; Abraham, K. M. *MRS Bull.* **2011**, *36*, 506−512.
(2) Ji, X.; Nazar, L. F. *J. Mater. Chem.* **2010**, *20*, 9821−9826.
(3) Manthiram, A.; Fu, Y.; Su, Y.-S. *Acc. Chem. Res.* **2012**, DOI: 10.1021/ar300179v.
(4) Sun, X.-G.; Wang, X.; Mayes, R. T.; Dai, S. *ChemSusChem* **2012**, *5*, 2079−2085.
(5) Shim, J.; Striebel, K. A.; Cairns, E. J. *J. Electrochem. Soc.* **2002**, *149*, A1321−A1325.
(6) Fu, Y.; Su, Y.-S.; Manthiram, A. *ACS Appl. Mater. Interfaces* **2012**, *4*, 6046−6052.
(7) Xin, S.; Gu, L.; Zhao, N.-H.; Yin, Y.-X.; Zhou, L.-J.; Guo, Y.-G.; Wan, L. J. *J. Am. Chem. Soc.* **2012**, *134*, 18510−18513.
(8) Wang, J.; Chew, S. Y.; Zhao, Z. W.; Ashraf, S.; Wexler, D.; Chen, J.; Ng, S. H.; Chou, S. L.; Liu, H. K. *Carbon* **2008**, *46*, 229−235.
(9) Su, Y.-S.; Manthiram, A. *Nat. Commun.* **2012**, DOI: 10.1038/ncomms2163.
(10) Cheon, S.-E.; Ko, K.-S.; Cho, J.-H.; Kim, S.-W.; Chin, E.-Y.; Kim, H.-T. *J. Electrochem. Soc.* **2003**, *150*, A796−A799.
(11) Cheon, S.-E.; Ko, K.-S.; Cho, J.-H.; Kim, S.-W.; Chin, E.-Y.; Kim, H.-T. *J. Electrochem. Soc.* **2003**, *150*, A800−A805.
(12) Mikhaylik, Y. V.; Akridge, J. R. *J. Electrochem. Soc.* **2004**, *151*, A1969−A1976.
(13) Yin, L.; Wang, J.; Lin, F.; Yang, J.; Nuli, Y. *Energy Environ. Sci.* **2012**, *5*, 6966−6972.
(14) Zhang, C.; Wu, H. B.; Yuan, C.; Guo, Z.; Lou, X. W. *Angew. Chem., Int. Ed.* **2012**, *51*, 9592−9595.
(15) Su, Y.-S.; Manthiram, A. *Chem. Commun.* **2012**, *48*, 8817−8819.
(16) Dörfler, S.; Hagen, M.; Althues, H.; Tübke, J.; Kaskel, S.; Hoffmann, M. J. *Chem. Commun.* **2012**, *48*, 4097−4099.
(17) Guo, J.; Xu, Y.; Wang, C. *Nano Lett.* **2011**, *11*, 4288−4294.
(18) Ji, L.; Rao, M.; Aloni, S.; Wang, L.; Cairns, E. J.; Zhang, Y. *Energy Environ. Sci.* **2011**, *4*, 5053−5059.
(19) Elazari, R.; Salitra, G.; Garsuch, A.; Panchenko, A.; Aurbach, D. *Adv. Mater.* **2011**, *23*, 5641−5644.
(20) Liang, C.; Dudney, N. J.; Howe, J. Y. *Chem. Mater.* **2009**, *21*, 4724−4730.
(21) Ji, X.; Lee, K. T.; Nazar, L. F. *Nat. Mater.* **2009**, *8*, 500−506.
(22) He, G.; Ji, X.; Nazar, L. *Energy Environ. Sci.* **2011**, *4*, 2878−2883.
(23) Zhang, B.; Qin, X.; Li, G. R.; Gao, X. P. *Energy Environ. Sci.* **2010**, *3*, 1531−1537.
(24) Jayaprakash, N.; Shen, J.; Moganty, S. S.; Corona, A.; Archer, L. A. *Angew. Chem., Int. Ed.* **2011**, *50*, 5904−5908.
(25) Schuster, J.; He, G.; Mandlmeier, B.; Yim, T.; Lee, K. T.; Bein, T.; Nazar, L. F. *Angew. Chem., Int. Ed.* **2012**, *51*, 3591−3595.
(26) Wang, H.; Yang, Y.; Liang, Y.; Robinson, J. T.; Li, Y.; Jackson, A.; Cui, Y.; Dai, H. *Nano Lett.* **2011**, *11*, 2644−2647.
(27) Ji, L.; Rao, M.; Zheng, H.; Zhang, L.; Li, Y.; Duan, W.; Guo, J.; Cairns, E. J.; Zhang, Y. *J. Am. Chem. Soc.* **2011**, *133*, 18522−18525.
(28) Evers, S.; Nazar, L. F. *Chem. Commun.* **2012**, *48*, 1233−1235.
(29) Zhang, F.; Zhang, X.; Dong, Y.; Wang, L. *J. Mater. Chem.* **2012**, *22*, 11452−11454.

(30) Xiao, L.; Cao, Y.; Xiao, J.; Schwenzer, B.; Engelhard, M. H.; Saraf, L. V.; Nie, Z.; Exarhos, G. J.; Liu, J. *Adv. Mater.* **2012**, *24*, 1176−1181.
(31) Fu, Y.; Manthiram, A. *J. Phys. Chem. C.* **2012**, *116*, 8910−8915.
(32) Yang, Y.; Yu, G.; Cha, J. J.; Wu, H.; Vosgueritchian, M.; Yao, Y.; Bao, Z.; Cui, Y. *ACS Nano* **2011**, *5*, 9187−9193.
(33) Wu, F.; Chen, J.; Li, L.; Zhao, T.; Chen, R. *J. Phys. Chem. C.* **2011**, *115*, 24411−24417.
(34) Wang, S.; Li, W.-C.; Hao, G.-P.; Hao, Y.; Sun, Q.; Zhang, X.-Q.; Lu, A.-H. *J. Am. Chem. Soc.* **2011**, *133*, 15304−15307.
(35) Hao, G.-P.; Li, W.-C.; Qian, D.; Wang, G.-H.; Zhang, W.-P.; Zhang, T.; Wang, A.; Schüth, F.; Bongard, H.; Lu, A.-H. *J. Am. Chem. Soc.* **2011**, *133*, 11378−11388.
(36) Han, F.; Li, W.-C.; Li, M.-R.; Lu, A.-H. *J. Mater. Chem.* **2012**, *22*, 9645−9651.
(37) Xin, S.; Guo, Y.-G.; Wan, L.-J. *Acc. Chem. Res.* **2012**, *45*, 1759−1769.
(38) Wang, Q.; Wang, W.; Huang, Y.; Wang, F.; Zhang, H.; Yu, Z.; Wang, A.; Yuan, K. *J. Electrochem. Soc.* **2011**, *158*, A775−A779.
(39) Wang, D.-W.; Zhou, G.; Li, F.; Wu, K.-H.; Lu, G. Q.; Cheng, H.-M.; Gentle, I. R. *Phys. Chem. Chem. Phys.* **2012**, *14*, 8703−8710.
(40) Han, F.; Li, D.; Li, W.-C.; Lei, C.; Sun, Q.; Lu, A.-H. *Adv. Funct. Mater.* **2012**, DOI: 10.1002/adfm.201202254.
(41) Sun, M.; Zhang, S.; Jiang, T.; Zhang, L.; Yu. *J. Electrochem. Commun.* **2008**, *10*, 1819−1822.
(42) Song, G.-M.; Li, W.-J.; Zhou, Y. *Mater. Chem. Phys.* **2004**, *87*, 162−167.